BABEȘ-BOLYAI UNIVERSITY

FACULTY OF PHYSICS

PHYSICS DOCTORAL SCHOOL

**PhD Thesis**

# Biopolymer-Based Composites for Soft Tissue Regeneration in Rats with Experimentally Induced Disease

**Scientific advisors:**

Prof. dr. Lucian BAIA
Prof. dr. Ionel PAPUC

**PhD Student:**

Elena-Alexandra FERARU

Cluj-Napoca

2026

## Table of Contents

# 1. Introduction

The consequences that acute or chronic wounds bring to the body have undesirable effects both in the short and medium term, as well as in the long term. Whether it is about replacing an affected part, improving certain functions, treating anomalies, or remediating some aesthetic aspects, tissue engineering has a fundamental role in the research and development of new approaches needed in wound management. The focus falls on materials with physical, chemical, and biological properties that can be easily manipulated so that they come as close as possible to the native tissue. In the current research context, biomaterials have stood out through a material-tissue interaction with the advantage of stimulating the regeneration process within the limit of minimal toxicity.

Many of the biomaterials, such as bioceramics, bioactive galsses, polymers, hydrogels and composites, have already been successfully investigated in many applications involving the healing of hard tissues, particularly bone tissue [1–3]. There has been a growing interest and challenge in the introduction of biomaterials for soft tissue reconstruction applications. Studies have shown that polymers, bioceramics or metal nanoparticles have potential in applications involving the regeneration or management of wounds in skin, cardiac, pulmonary, muscle or nervous tissues. But the field is still in full development, because compared to hard tissue, soft tissues need different biochemical and biomechanical properties, which requires new approaches in the synthesis and characterization of future tissue substitutes.

Volumetric muscle loss (VML) is a severe form of skeletal muscle trauma, characterized by the loss of a significant amount of muscle tissue, which exceeds the body's natural regeneration capacity. This type of injury cannot be effectively repaired by normal physiological mechanisms alune, as it affects not only muscle fibers, but also the

extracellular matrix, vascular network and local innervation, leading to extensive scar formation and irreversible functional loss. Recent advances in the field of biomaterials for the treatment of VML have been highlighted by the development of biomimetic scaffolds from biodegradable natural or synthetic materials, 3D bioprinting, or the introduction of growth factors [4–6].

This study provides a reproducible animal model for investigating VML and highlights the therapeutic potential of a scaffold-based regenerative medicine approach. The targeted implantation of composite biopolymeric scaffolds within the defect was associated with constructive tissue remodeling, including the formation of site-specific skeletal muscle tissue.

## 1.1 Aim of the Ph.D. thesis

The aim of this thesis was focused on the synthesis of biopolymer composites with applications in soft tissue engineering regeneration. For this purpose, three biopolymers were selected – Na-Alg, GA and MCC. To obtain efficient materials for regenerative engineering applications, biopolymer systems were modified with inorganic agents, namely, spherical cerium oxide nanoparticles ($CeO_2$ NPs), $SiO_2$-CaO-$P_2O_5$ (BG) and gold nanoparticle doped bioactive glass (BGAuSP). The structural and morphological characteristics of the synthesized materials were investigated in detail by specific techniques.

## 1.2 Objectives of the thesis

a. Using Na-Alg and GA as main materials, in which $CeO_2$ NPs were subsequently introduced into the polymer matrix to obtain porous cryogels.

- optimizing the ratio between the two polysaccharides
- solvothermal synthesis of $CeO_2$ NPs
- preparation of gels, using three concentrations of $CeO_2$ NPs

- obtaining porous structures through the two steps lyophilization process
- external crosslinking of matrix in the presence of $Ca^{2+}$ cations
- in vitro evaluation to certify bioactivity and eliminate the risk of forming toxic compounds
- characterization of morphological, structural, thermal properties, porosity, in vitro bioactivity, biodegradation, and swelling ratio

b. Using Na-Alg and microcrystalline celullose as main materials, in which BG and BGAuSP were subsequently introduced into the polymer matrix to obtain porous cryogels.

- optimizing the ratio between the two biopolimers
- synthesis by sol-gel method of BG and BGAuSP
- preparation of gels, using different concentrations of inorganic agents
- internal crosslinking of matrix in the presence calcium carbonate ($CaCO_3$) and D-(+)-gluconic acid δ-lactone (GDL)
- obtaining porous structures through the lyophilization process
- in vitro evaluation to certify bioactivity and eliminate the risk of forming toxic compounds
- characterization of morphological, structural, thermal properties, porosity, in vitro bioactivity, biodegradation, and swelling ratio

c. In vivo evaluation in animal model to assess the efficacy and safety of polymeric biomaterials and to investigate the performance of composites in promoting volumetric muscle loss.

- choosing the animal model depending on its relevance and compatibility with the materials studied

- highlighting all the properties demonstrated in objective no. 1, in vivo by implanting porous scaffolds
- highlighting the changes brought to the animal body through histopathological examinations

## 1.3 Outline and structure of the PhD thesis

The present doctoral thesis entitled "Biopolymer-Based Composites for Soft Tissue Regeneration in Rats with Experimentally Induced Disease" addresses the synthesis and characterization of polymer matrices based on biopolymers (Alg, GA, MCC) in which oxide nanoparticles ($CeO_2$) and bioactive constituents (BG and BGAu) have been incorporated in order to evaluate in vitro and in vivo behavior with the aim of use in soft tissue engineering applications. The doctoral thesis is structured in 4 chapters, each with related subchapters and their conclusions, a chapter addressed to general conclusions and future research perspectives, bibliographic references, a list of published works, dissemination of results in national and international scientific events and awards obtained.

**Chapter 1** briefly presents the anatomy of muscles, which are composed of multinucleated muscle fibers, satellite cells (responsible for regeneration), extracellular matrix, and a complex vascular and neural network. This is followed by an introduction to muscle tissue engineering, with a focus on the used biomaterials that aim to mimic structural and functional components and to provide both mechanical and biological support for regeneration.

**Chapter 2** highlights the current state of knowledge in the field of biopolymers and composites used in muscle regeneration as well as the general and specific objectives of this work.

**Chapter 3** presents the scientific contributions, in the form of scientific articles, divided into 3 subchapters, each detailing the in vitro and in vivo investigations used to investigate the composites proposed in the previous chapter.

**Chapter 4** is addressed to the final conclusions and perspectives of the studed topics as well as to the personal contribution to the development of the doctoral thesis.

# 2. Methods and characterization of the materials

## 2.1 Fourier Transform Infrared Spectroscopy (FT-IR)

The FT-IR absorption spectra were recorded in reflection configuration with a Jasco 6600 (Jasco, Tokyo, Japan) spectrometer using the well-known KBr pellet technique and the following parameters: room temperature, 400–4000 $cm^{-1}$ spectral range, and 4 $cm^{-1}$ spectral resolution.

## 2.2 Raman Spectroscopy

Raman spectra were recorded with a multilaser confocal Renishaw in via Reflex Raman spectrometer, equipped with a RenCam CCD detector and 1800 lines/mm grating. Raman spectra were collected by using a 0.9 NA objective of 100× magnification. As an excitation source, the 532 nm laser was employed. The spectral resolution was of approximately 4 $cm^{-1}$.

## 2.3 Solid-State Nuclear Magnetic Resonance Spectroscopy (NMR)

Solid-state 1H NMR spectra were recorded under Magic Angle Spinning (MAS) conditions with an Avance III 500 wide bore (WB) Bruker spectrometer at 11.7 Tesla applied magnetic field. The spinning sidebands free 1H MAS spectra of the central transition were obtained while engaging a 1.3 mm diameter rotor/sample holder spun at 50 kHz frequency. The 1H MAS NMR chemical shifts were referenced to solid state adamantane (1.8 ppm). The single pulse sequence was employed, and a total of 8 scans

were accumulated with 5 s relaxation delay. The 90-degree pulse was obtained after a 1.25 us and a power level of 31.62 W. The time domain was set at 2048.

## 2.4 X-ray Diffraction (XRD)

XRD patterns were obtained from pure and hybrid composites using CuK$\alpha$ radiation ($\lambda$ = 1.54 Å) and Ni filter (Shimadzu XRD 6000 diffractometer, Kyoto, Japan). XRD analyses were conducted in the 2θ range 10°–80° with a scan speed of 2 °/min.

## 2.5 Thermogravimetric Analysis (TGA) and Differential Thermal Analysis (DTA)

The thermogravimetric analyses were performed with Shimadzu DTG-60H (Shimadzu, Japan) instrument, which recorded the DTA curves as the difference between the temperature of the sample to be analyzed and the alumina standard sample, and the TG curves as a change in the weight of the sample depending. All measurements were recorded in a $N_2$ atmosphere with a flow rate of 70 mL·min−1. Heating rates of 10 °C min−1 were adopted, with a temperature range between 25–600 °C, using alumina crucibles for the samples with masses of approximately 9 mg.

## 2.6 Transmission Electron Microscopy (TEM)

The shape and morphology of the nanoparticles were observed by TEM. The micrographs were analyzed by FEI Technai G2 F20 high-resolution transmission electron microscope (Philips CM 10 instrument, Amsterdam, Netherlands) equipped with 200 kV, W cathode. The samples were suspended in bidistilled water and dropped on a 300 mesh Cu grid. The obtained images were interpreted with ImageJ software.

## 2.7 UV-Vis Diffuse Reflectance Spectroscopy (UV-Vis DRS)

Th UV–Vis DRS measurements were carried out on a Jasco-V780 UV–Vis spectrophotometer (Tokyo, Japan) equipped with an ILV-724 integrative sphere, in the wavelength range from 190 to 800 nm.

## 2.8 Zeta potential

A Malvern Nano ZS90 Zetasizer particle analyzer equipped with a Hesingle bondNe laser (633 nm, 5 mW) was used to examine the zeta potential of samples in a water suspension. Each investigation consisted of five sets of 30 measurements, all taken at a scattering angle of 90 deg. and at a temperature of 25 C°. The laser attenuation level for each measurement was chosen automatically by the software.

## 2.9 Scanning Electron Microscopy (SEM)

The topography of the cryogels was examined using SEM. All micrographs were analyzed by a Hitachi S-4700 Type II cold field emission SEM (Tokyo, Japan) operating at an acceleration voltage of 10 kV.

## 2.10 Inductively Coupled Plasma-Optical Emission Spectrometry (ICP-OES)

The Ce, Ca, and P content were determined using Optima 5300 DV (Perkin-Elmer, Woodbridge, ON, Canada) inductively coupled plasma-optical emission spectrometer (ICP-OES). Approximatively 65 mg sample was digested with aqua regia (HCl 37 %: HNO3 65 %, 3:1, v:v) in in closed polytetrafluoroethylene vessel using a microwave Speedwave Xpert system (Berghof, Eningen, Germany). The digested samples were filtered and diluted to 20 mL with ultrapure water (Elga PURELAB flex, Veolia, Wycombe, UK).

## 2.11 Porosity

The porosity of the samples was calculated using the density theory (Equation 2.11.1) and the liquid displacement method (Equation 2.11.2). The density theory method involves the calculation of two values for the density of the composites, the apparent density being defined as the ratio between the real mass and the volume of the composites, and the second one representing the theoretical density (Equation 2.11.3)

of the raw materials. The volume was calculated as the average dimensions of the three dry samples.

$$P = \left(1 - \frac{\rho_{apparent}}{\rho_{theoretic}}\right) \times 100(\%) \quad (2.11.1)$$

$$\rho_{apparent} = \frac{w}{V} \quad (2.11.2)$$

$$\rho_{theoretic} = \frac{1}{\frac{w_{GA}}{\rho_{GA}} + \frac{w_{Alg}}{\rho_{Alg}}} \quad (2.11.3)$$

where the $\varrho_{GA}$ and $\varrho_{Alg}$ values were provided by the supplier.

For the liquid displacement method [7] ethanol was used as displacement liquid, and the percentage of porosity was calculated according to the following formula:

$$P(\%) = \left[\frac{W_1 - W_0}{\rho_{EtOH} \times V_0}\right] \times 100 \quad (2.11.4)$$

where $W_0$ is the dry weight of the composite, $W_1$ is the weight of the composite saturated with ethanol, $\varrho_{EtOH}$ is the density of the ethanol, and $V_0$ is the initial volume of the composite scaffold.

## 2.12 In Vitro Degradation and Mineralization

Controlled in vitro hydrolytic degradation experiments were carried out by immersion of cylindrical polymer structures (length = 8 mm and diameter = 5 mm) in 10 mL of SBF solution at pH 7.4 at a temperature of 37 °C. At regular time intervals (1, 3, 5, 7, and 14 days), the samples were removed and rinsed with ultrapure water. After weighing, they were dried for 48 h at 37 °C. The water uptake (Equation 2.12.1) and weight loss (Equation 2.12.2) were calculated according to the following formulas:

$$\text{Water uptake} = \left(\frac{Ws - Wd}{Wd}\right) \quad (2.12.1)$$

$$\text{Weight loss} = \left(\frac{W0 - Wd}{W0}\right) \times 100 \quad (2.12.2)$$

$W_0$—initial weight; $W_s$—swollen weight; and $W_d$—dry weight

## 2.13 Synthesis Cryogel Composites

### 2.13.1 Synthesis of Alg–GA cryogel composites

Porous cryogels were prepared following two lyophilization cycles, each lasting 24 h. Lyophilization was carried out at −55 °C using a Vacuum Freeze Dryer (BK-FD 10 Series, Biobase Biodustry, Shandong Co., Ltd., Jinan, China). Before each cycle of freeze-drying, the samples were frozen at −18 °C for 24 h. The composites' preparation process was completely based on the ionic cross-linking method. Briefly, a sodium alginate solution (*w*/*v*) was prepared by dissolving the powder in 8 mL of ultrapure water for 1 h under mechanical stirring to completely dissolve the alginate. For the alginate–gum arabic composites, the gum arabic solutions with weight ratios 10 *w*/*v*, 16 *w*/*v*, and 26 *w*/*v* (Alg-10GA, Alg-16GA, and Alg-26GA, respectively) were added to the mixture of alginate and stirred for 1 h until the solution became viscous and homogeneous. Prior to the first lyophilization cycle, the obtained composites were gently poured into a 96-well plate and refrigerated for 24 h. Subsequently, they were immersed in a $CaCl_2$ solution, which was used as a cross-linker agent, for 4 h. After that, the samples were rinsed gently with ultrapure water and stored in the freezer before the lyophilization process was repeated.

### 2.13.2 Synthesis of AlgGA-$CeO_2$ *cryogel composites*

The hydrogel formation and nanoparticle inclusion with a concentration of 0; 0.3; 0.65 and 1 wt% abbreviated as AlgGA; AlgGA-0.3$CeO_2$; AlgGA-0.65$CeO_2$; AlgGA-1$CeO_2$ was prepared by the ionic crosslinking method, in two lyophilization stages. The composites concentration was 3 % *w*/w, where the alginate: gum arabic weight ratio is 85:15. Alginate and gum arabic solutions were prepared separately by dissolving the powders in ultrapure water under magnetic stirring for 1 h at room temperature. Simultaneously, each concentration of $CeO_2$NPs was prepared as a colloidal solution in 1 mL of ultrapure water and sonicated for 1 h. After complete dissolution, the two polysaccharides were

mixed, then $CeO_2$NPs were added, and magnetic stirring was maintained for another 30 min until a homogeneous viscous solution was obtained. The resulting gel was immediately poured, by pipetting, into a 96-well plate and refrigerated for 24 h at −4 °C. After complete freezing, the samples were lyophilized for 24 h. To stabilize the polymer matrix, the porous cryogels were removed from the well plate and ionically cross-linked by immersion in $CaCl_2$ solution (4 %) for 4 h. In the final step, the samples were gently washed with Milli-Q water, frozen, and then lyophilized a second time.

### 2.13.3 Synthesis of BG-Alg-MCC and BGAuSP-Alg-MCC cryogel composites

The composite synthesis was based on the ionic cross-linking method. The 1.5 % (*w*/*v*) sodium alginate (Na-Alg) and MCC polymeric solutions were dissolved in ultrapure water (25 mL) under continuous stirring. To the alginate-cellulose solution, 5 mL of calcium carbonate ($CaCO_3$) with a concentration of 112.5 mM was added. The mixture was continuously stirred until homogenization (30 min). The bioactive glasses (BG and BGAuSP) were ultrasonicated for 1 h to obtain a uniform particle size, then added to the polymeric solution. To initiate the ionization of $CaCO_3$, 5 mL D-(+)-gluconic acid δ-lactone (GDL) solution was added to the mixture, and the solution was immediately poured into the well plate. The weight ratio of the Alg-MCC composite was 1:0.15. As a reference, a pure alginate (Alg) sample was prepared. The bioactive glasses were added to the polymeric mixture in a weight ratio of 12 wt% and abbreviated as BG-Alg-MCC and BGAuSP-Alg-MCC.

## 2.14 Animal care and ethics

This study was conducted in compliance with the Animal Welfare Act, all procedures being approved by the Regional Sanitary Veterinary and Food Safety (nr. 369/13.06.2023), and in accordance with the principles of the Guide for the Care and Use of Laboratory Animals. The guidelines of Directive 63/2010/EU were adapted from National Law

43/2014. Adult male, one-year-old, Wistar rats (300 g body weight) obtained from an authorized breeding unit (Cantacuzino Institute, Bucharest, Romania) were housed in individual standard cages, maintained with a 12-h light/dark cycle, in the authorized Laboratory Animal Facility (University of Agricultural Science and Veterinary Medicine, Cluj-Napoca). Animals had free access to standard rodent food and water throughout the study.

### 2.14.1 Surgery protocol

The surgical site (left hind limb) was aseptically prepared (Figure 2.14.1). The right hind limb was kept as an internal control. A lateral incision just below the knee was made through the skin to reveal the tibialis anterior (TA) muscle (Figure 2.14.1A). The injury to the TA muscle was created by a 6 mm punch biopsy (Kai Medical) to remove approximately ~20% of the muscle mass (Figure 2.14.1B and C). A subset of injured animals was treated with BGAuSP-Alg-MCC hydrogel composites (n = 10 per group), while the remaining subset was left untreated (n = 10 per group). This material was selected for its unique combination of non-toxic components and enhanced bioactivity. It was regarded as the most complex synthesis, likely yielding the desired biological effects. Bleeding was controlled with light pressure, and the fascia and skin were closed using vicryl (6–0) and prolene (6–0) interrupted sutures. A compression bandage was then wrapped around the lower leg for 5–10 min. The animals were humanely euthanized via prolonged narcosis via isoflurane, followed by cervical dislocation, and the TA muscles were harvested at 14 and 30 days.

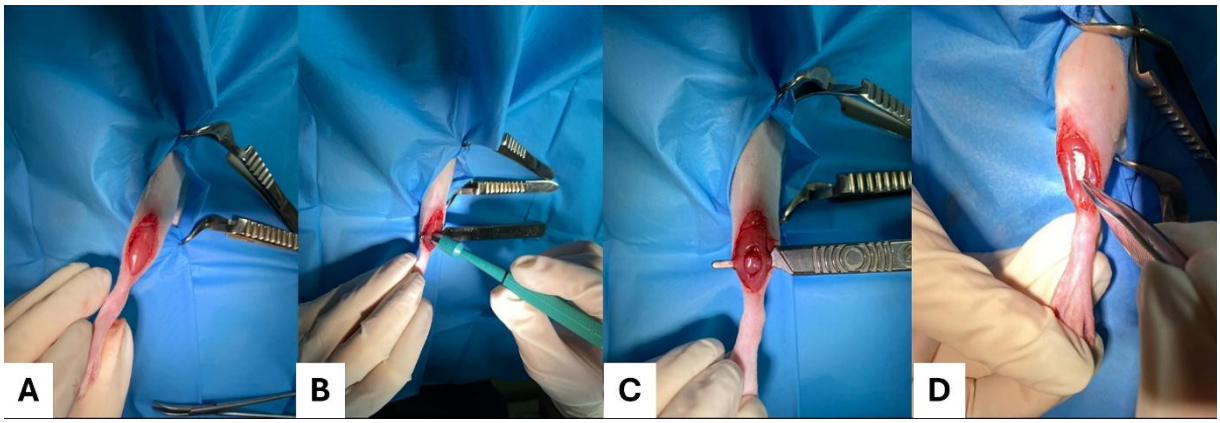


Figure 2.14.1 VML standard experimental defect. The VML model consists of a 6 mm full-thickness surgical defect to the middle third of the TA muscle of male Wistar rats (A-C). The treatment involves applying biomaterial for the regeneration of volumetric muscle loss in muscle injuries (D) [8].

# 3. Results and Discussions

## 3.1 Anionic Polysaccharide Cryogels: Interaction and In Vitro Behavior of Alginate–Gum Arabic Composites

The paper investigates biopolymer cryogels based on sodium alginate and gum arabic, two anionic polysaccharides with biomedical significance. The goal was to synthesize and characterize cryogels with varied gum arabic content to explore their structural interactions, mechanical properties, bioactivity, and potential biomedical applications—including tissue engineering and wound management.

**Cross-Linking of the Alginate–Gum Arabic Cryogel Composites**

Spectroscopic investigations showed that ionic cross-linking is the dominant mechanism linking alginate and gum arabic in the presence of $Ca^{2+}$ ions. A notable shift and intensity change in symmetric and asymmetric –COO– stretching bands in FT-IR confirmed the ionic interactions between the carboxyl groups of both polysaccharides (Figure 3.1.1).

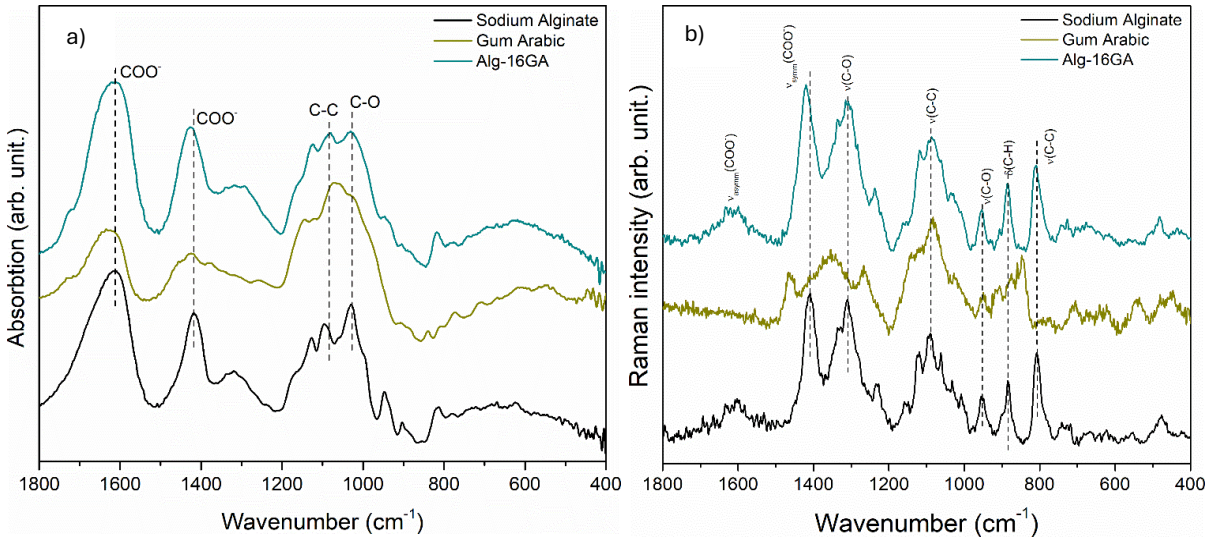


Figure 3.1.1 FT-IR (a) and Raman spectra (b) of pure Alg (black line), pure GA (yellow line), and cross-linked Alg-16GA composite (green line) [9].

Additionally, MAS NMR (Figure 3.1.2) and Raman spectroscopy further supported that the two polymers form a chelating, interconnected network (Figure 3.1.3).

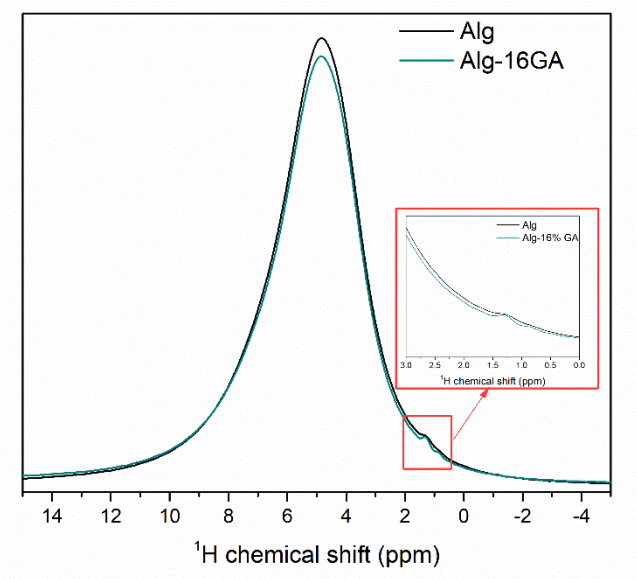


Figure 3.1.2 1H-NMR spectra of the Alg and Alg-16GA composite. The insert graph shows the enlarged part of the 1H-NMR spectra [9].

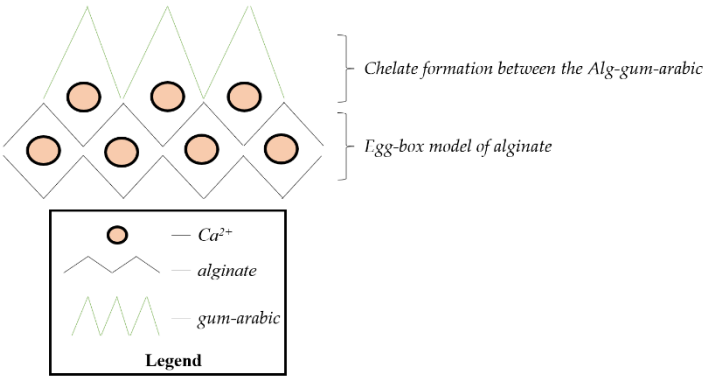


Figure 3.1.3 Proposed cross-linking mechanism of the Alg–GA biopolymers [9].

**Morphological Results**

SEM imaging (Figure 3.1.3) revealed that all cryogels exhibited high porosity (≈ 80–90%) with an interconnected network—an architecture favorable for tissue engineering due to enhanced cell infiltration and nutrient transport. Increasing gum arabic content led to smaller, more defined pores, creating a more uniform and organized structure. In contrast, samples with low or no gum arabic showed irregular and wider pores. This indicates that gum arabic not only influences mechanical properties but also regulates microarchitecture critical for biomaterial performance.

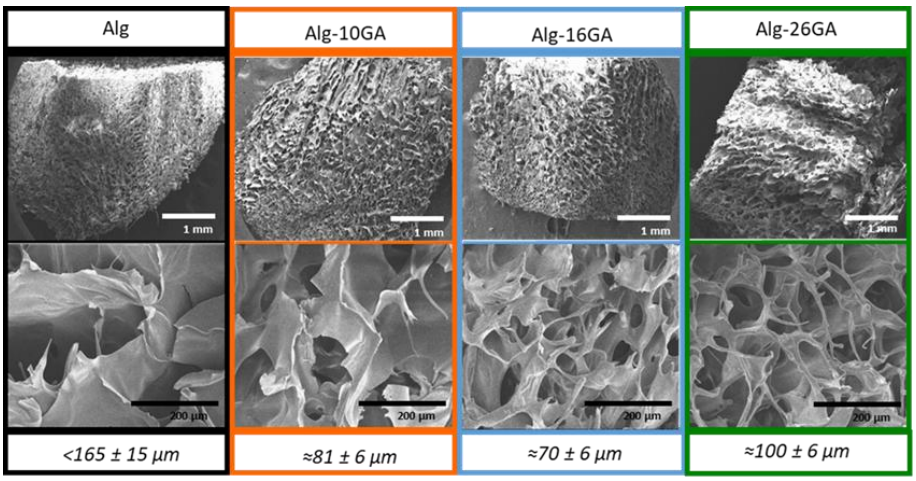


Figure 3.1.3 SEM micrographs of cross-linked Alg–GA composites with 1 mm and 200 µm magnifications [9].

**Bioactivity and Mineralization**

One of the key results was the development of an apatite layer on the cryogel surfaces after prolonged immersion in simulated body fluid. The layer's morphology evolved toward a cauliflower-like structure — a hallmark of bioactive behavior. XRD and SEM analyses indicated the presence of stable calcium phosphate phases, with a trace amount of calcium oxalate, reflecting mineral formation similar to bone minerals.

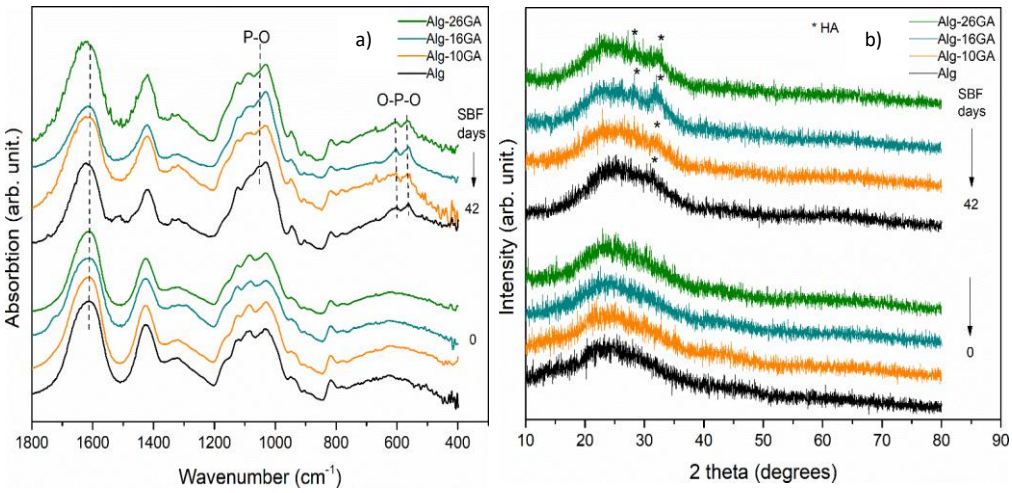


Figure 3.1.4 FT-IR spectra (a) and XRD patterns (b) of Alg-xGA (x = 0, 10, 16, and 26 wt.%) composites, before and after immersion in SBF up to 42 days [9].

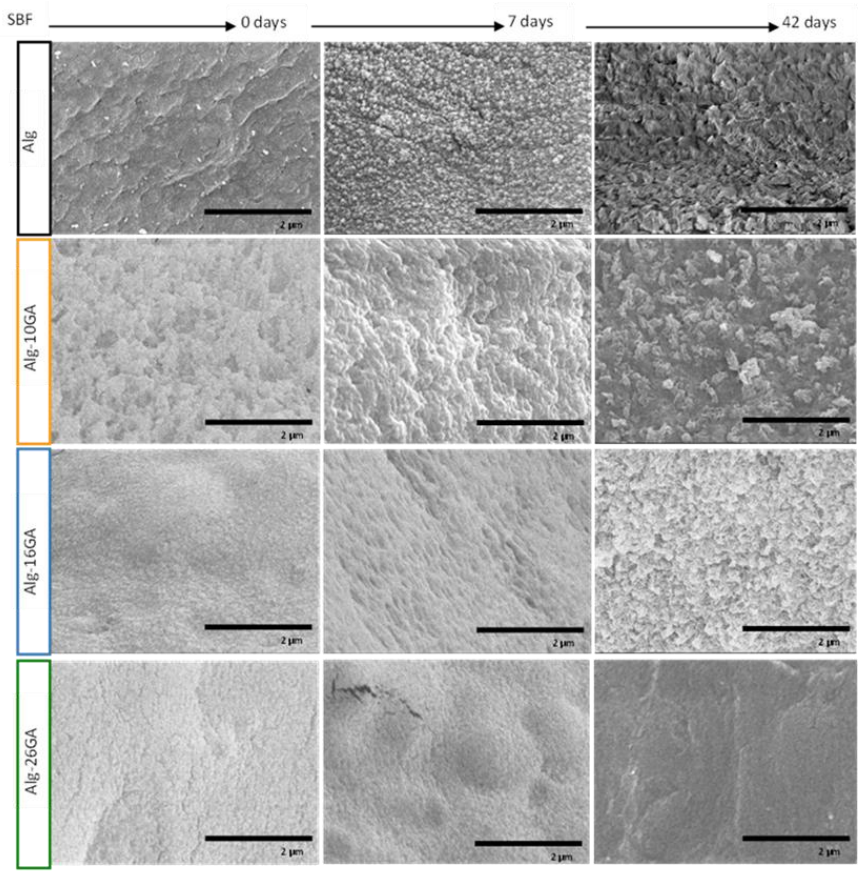


Figure 3.1.5 SEM micrographs of cross-linked Alg–GA composites, before and after immersion in SBF for 7 and 42 days [9].

Interestingly, the degree of crystallinity increased with gum arabic content, especially in samples with moderate ratios of gum arabic compared to alginate alone. This suggests that the presence of gum arabic facilitates mineral nucleation and growth, a desirable property for scaffolds intended for bone or tissue regeneration.

**Water Uptake and Degradation**

Swelling tests revealed that cryogels rapidly absorbed water within the first days of immersion, reaching equilibrium by ~5 days. The water uptake capacity was influenced by gum arabic content, with higher ratios showing larger swelling and indicating more accessible pore networks and hydrophilic –OH and –COO– groups.

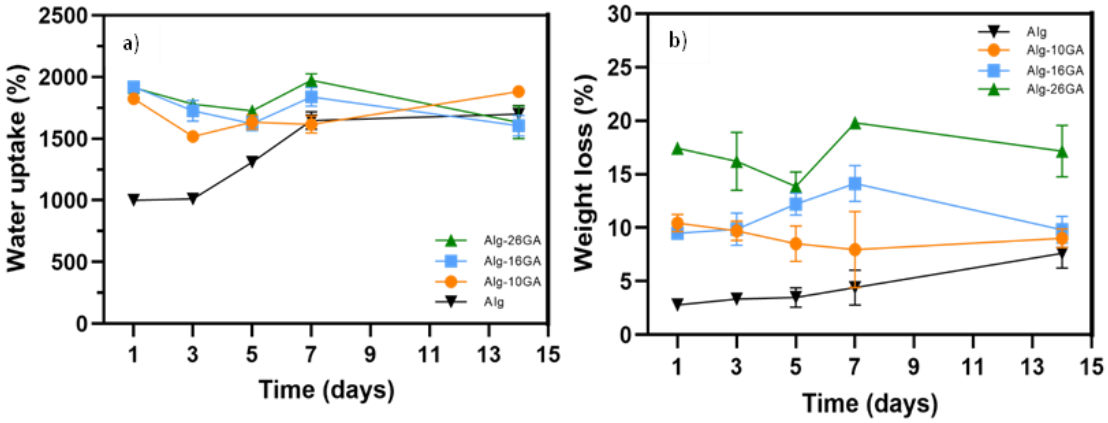


Figure 3.1.6 Water uptake (a) and degradation behavior (b) of Alg-xGA (x = 0, 10, 16, and 26 wt.%) composites [9].

**Cytotoxicity and In Vitro Compatibility**

Fibroblast cell assays demonstrated that all alginate–gum arabic cryogel composites were non-toxic, maintaining high cell viability after 24 hours. This supports biocompatibility and suggests that these materials could safely support cellular attachment and proliferation in wound or tissue engineering contexts.

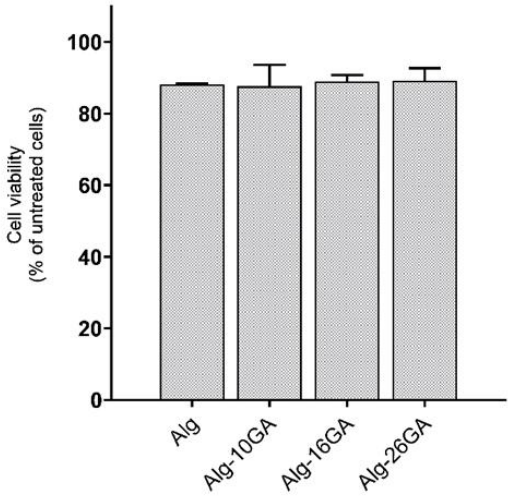


Figure 3.1.7 Viability of Hs cells after 24 h in the presence of Alg-xGA (x = 0, 10, 16, and 26 wt.%) composites [9].

**Conclusions**

Alginate and gum arabic can be co-crosslinked via ionic mechanisms in the presence of $Ca^{2+}$ to produce stable cryogels. Gum arabic significantly influences cryogel morphology, flexibility, swelling behavior, and bioactivity. Cryogels exhibit high bioactivity as evidenced by apatite formation and favorable mineralization in vitro. Biocompatibility tests confirm non-toxic behavior and potential for biomedical use.

## 3.2 The effect of nanoceria on the alginate-gum arabic crosslinking mechanism and in vitro behavior as a wound dressing

The research investigates how cerium oxide nanoparticles (nanoceria) affect the crosslinking behavior of an alginate–gum arabic polymeric wound dressing, and how this influences *in vitro* physical, chemical, and biological properties relevant to tissue repair. The work positions the composite cryogels as potential advanced wound dressings with enhanced antioxidant and regenerative capabilities compared to conventional materials.

**Cross-linking analysis of the composites**

Spectroscopy analyses revealed that nanoceria particles interacted with alginate and gum arabic chains, potentially by forming additional ionic or coordination bonds, which altered the crosslinked network configuration. By adding the $CeO_2$NPs to the composite, the band given by the carboxylate ion ($COO^-$) group at 1425 $cm^{-1}$ shifts to 1418 $cm^{-1}$. This indicates the participation of the hydroxyl group from nanoparticles in the bond formation within the polymeric matrix. In addition, the spectral changes identified by different ratios of the intensities and the shape of the bands in the range 1000–800 $cm^{-1}$ suggest that the polymeric matrix-nanoparticle system prefers to interact through the O − H and −COO functional groups [10]. The $CeO_2$ bands were not clearly distinguished in the FT-IR and Raman spectra of the composites because the characteristic bands overlapped with the polymer bands.

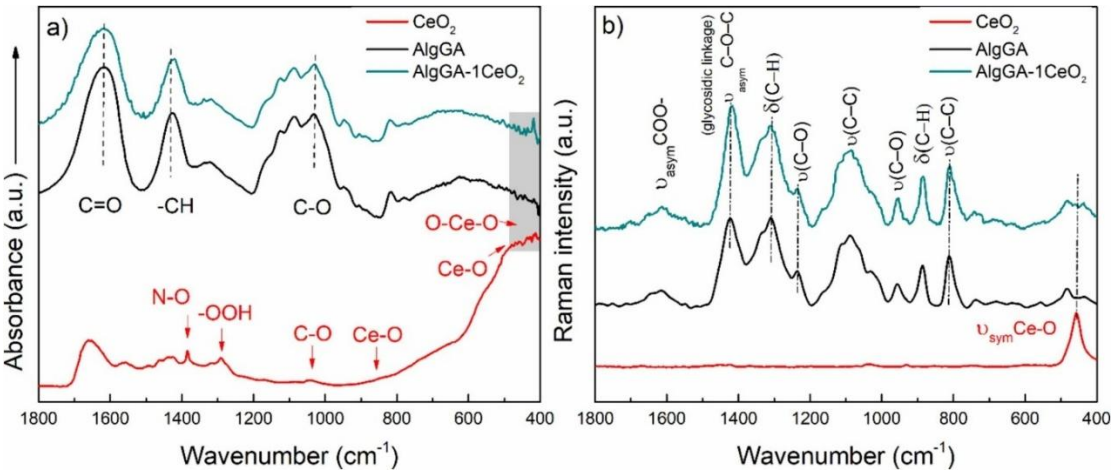


Figure 3.2.1 FT-IR (a) and Raman spectra (b) of $CeO_2$NPs (red line), cross-linked AlgGA (black line), and AlgGA-1$CeO_2$ (dark cyan line) composites [11].

To support these findings, UV–Vis spectroscopic and XRD measurements were performed. Figure 3.2.2a depicts the DRS-UV–Vis absorption spectra of $CeO_2$NPs and AlgGA-1$CeO_2$ porous cryogels. It was evident that the $CeO_2$NPs are characterized by an absorption band located at 362 nm. Noticeably, the electronic spectrum of AlgGA-$CeO_2$ porous cryogels shows intense absorption in the UV range, especially in the UVA (320–400 nm) region, indicating that the polymeric matrix retained the optical properties of the nanoparticles [12].

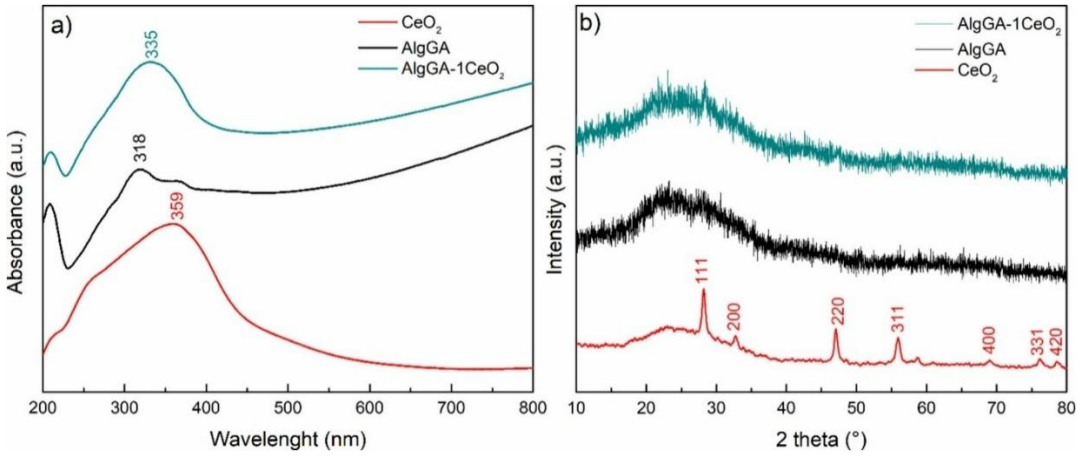


Figure 3.2.2 DRS UV–Vis spectra (a) and XRD patterns (b) of the $CeO_2$NPs (red line), cross-linked AlgGA (black line), and AlgGA-1$CeO_2$ (dark cyan line) composites [11].

The XRD pattern of the AlgGA composite recorded a broad peak at 2θ = 20–30° characteristic for the polymer matrix and indicates the amorphous nature of the composite (Fig. 3.2.2b). The reflections at 2θ = ≈28° and ≈47° that are noticed for the AlgGA-1$CeO_2$ sample are attributed to the (111) and (220) crystallographic planes specific to nanoceria.

The cerium could play the cross-linker role by exchanging the $Ca^{2+}$ cations. Adding $Ce^{4+}$ cation in the system could be a much stronger combination, with a higher coordinative number of the cerium cations than the calcium cations.

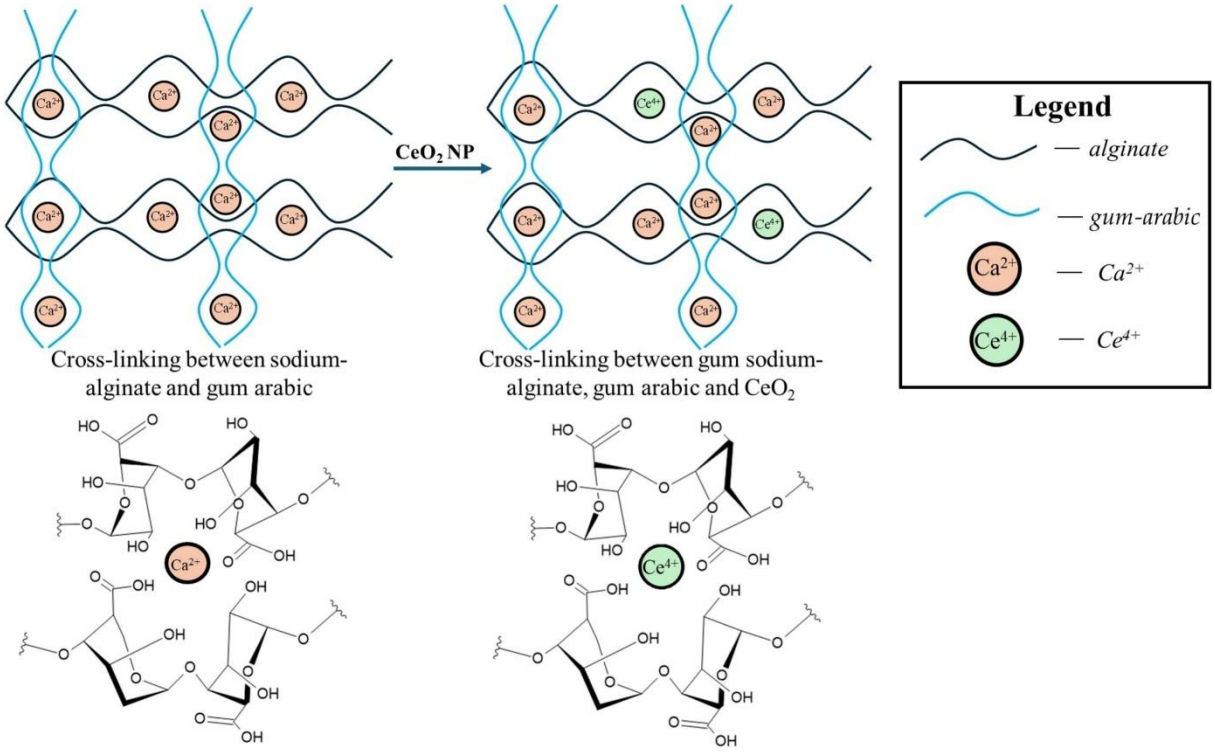


Figure 3.2.3 Proposed cross-linking mechanism of the Alg-GA $CeO_2$NPs [11].

**Characterization of the morphology and porous structure**

Cryogel scaffolds exhibited a highly porous, interconnected structure (macro- and micropores) favorable for fluid exchange and cell migration. The presence of nanoceria

resulted in more uniform pore distribution and modified wall thickness in the polymer matrix.

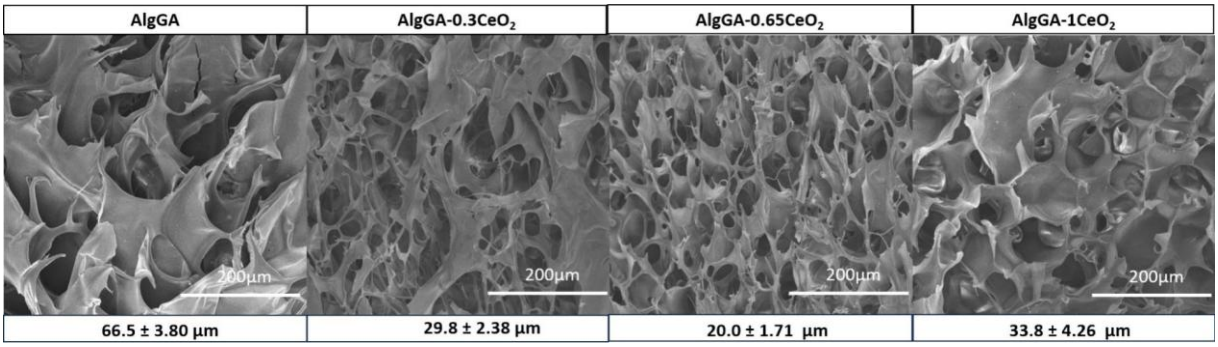


Figure 3.2.4 SEM micrographs of AlgGA, AlgGA-0.3$CeO_2$, AlgGA-0.65$CeO_2$; and AlgGA-1$CeO_2$ composites. Scale bar: 200 µm [11].

According to the liquid displacement method, the results show a porosity value of 94 % for the control sample, followed by a slight increase for the rest of the samples AlgGA-0.3$CeO_2$ (98 %), AlgGA-0.65$CeO_2$ (96 %) and AlgGA-1$CeO_2$ (97 %). The following study has pointed out that a porosity higher than 80 % is ideal when sponge-like structures are used as cellular scaffolds [12].

**In vitro behavior of the composites**

FT-IR analysis revealed a progressive increase in the intensity of the band at 1044 $cm^{-1}$ relative to the 1618 $cm^{-1}$ band, along with the appearance of a characteristic doublet at 561–620 $cm^{-1}$. These spectral features indicate the formation of hydroxyapatite on the sample surface, associated with phosphate precipitation. This process is attributed to the calcium ions used as crosslinking agents, which promote apatite nucleation and growth while reducing hydroxyl and carboxyl functional groups.

X-ray diffraction analysis showed that the initially amorphous biopolymer structure evolved into a semi-crystalline phase after immersion, with apatite reflections observed at approximately 26° and 33° (2θ). The moderate intensity of these peaks suggests low

apatite crystallinity at early stages. Extended immersion for up to 42 days confirmed sustained apatite growth without the formation of toxic compounds, thereby validating the bioactivity and safety of the materials.

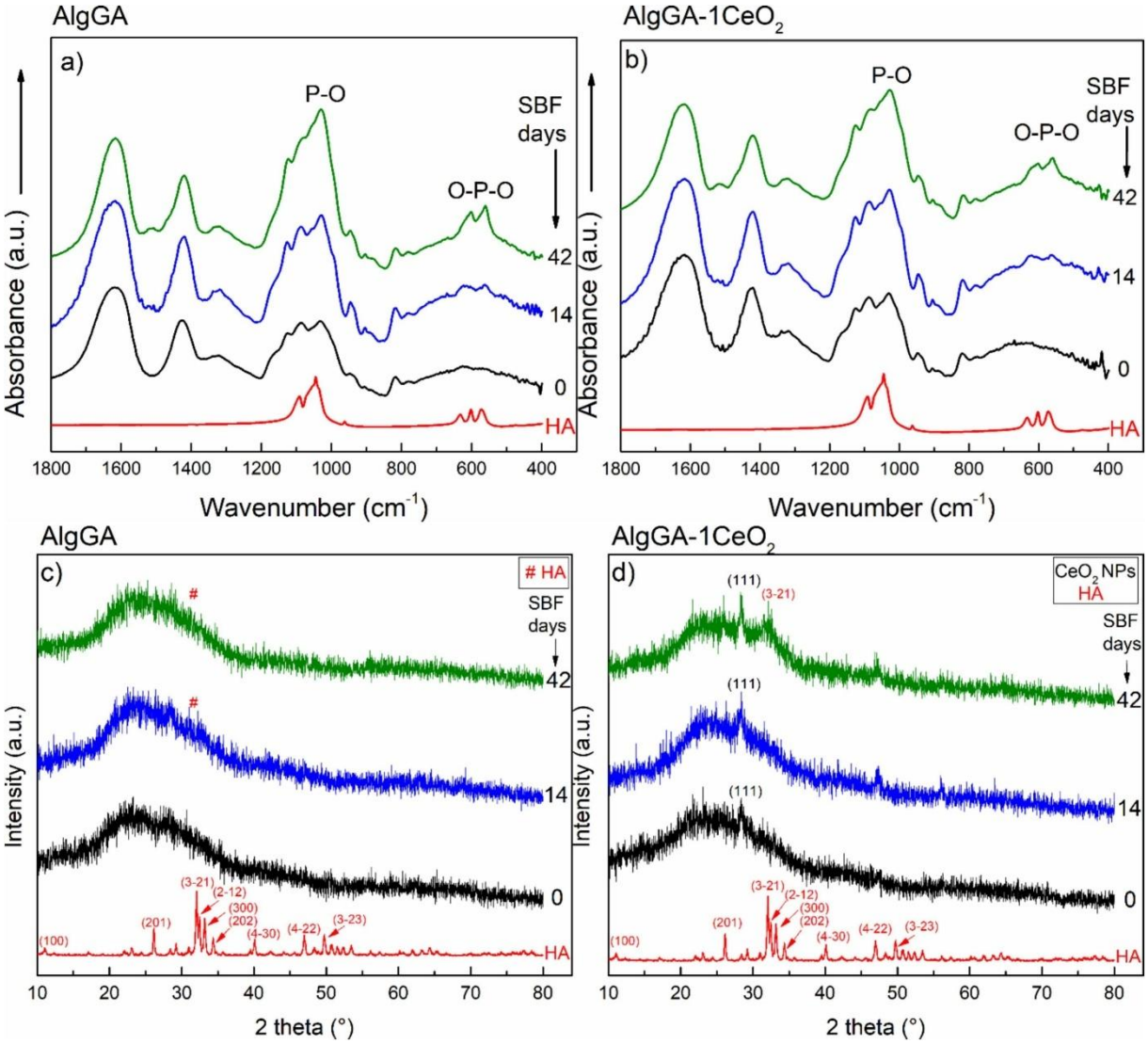


Figure 3.2.5 FT-IR spectra (a, b) and XRD pattern (c, d) of the AlgGA (a, c) and AlgGA-1$CeO_2$ (b, d) composites before (black line) and after 14 (blue line) and 42 immersion days (green line). The FT-IR spectrum and XRD pattern of HA (red line) were inserted for comparison purposes [11].

**In Vitro Cell Viability**

Keratinocytes and fibroblasts cultured on the composites showed high viability, confirming in vitro biocompatibility (Figure 3.2.5). Nanoceria release was gradual and coincided with polymer degradation, supporting sustained biological activity without acute cytotoxicity. The antioxidant environment created by nanoceria favored cell attachment and proliferation.

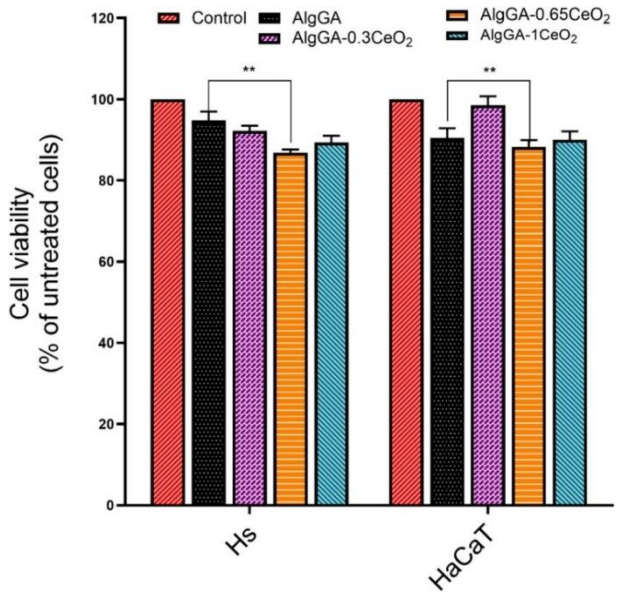


Figure 3.2.5 Cell viability of Hs and HaCaT cells following 24 h in contact with composites. The average cell viability obtained after testing in triplicate was used to compare the results to the control (untreated cell cultures). The results are expressed as the mean ± S.D. (n = 3), $P < 0.05$ [11].

The scratch assay was done to evaluate the wound healing ability in the first 24 h (Figure 3.2.6). The largest uncovered area was obtained for AlgGA composite. The presence of $CeO_2$NPs in the composites results in faster wound healing, obtaining a better value to AlgGA-0.65$CeO_2$ composite.

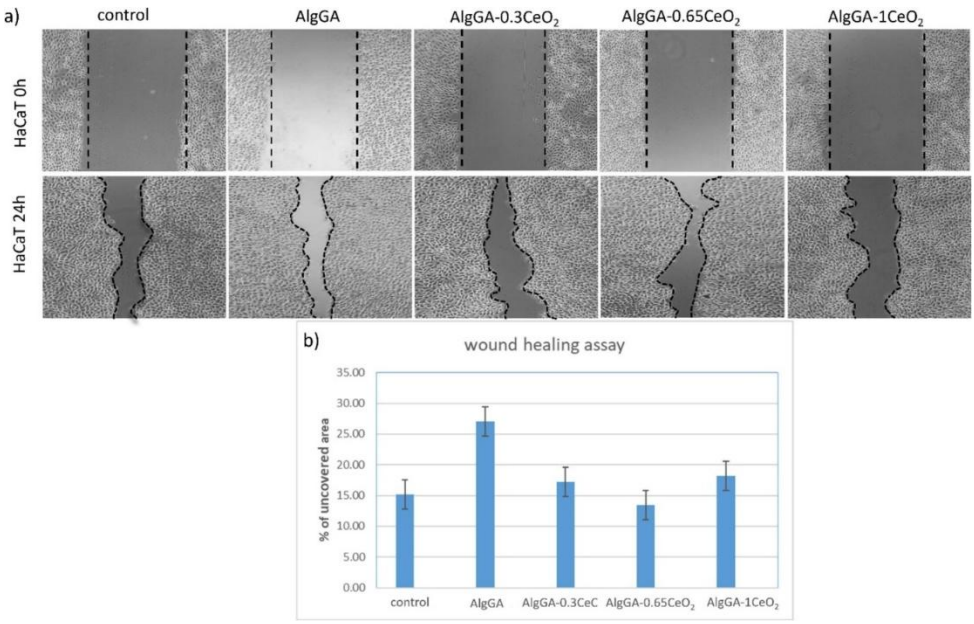


Figure 3.2.6 In vitro scratch wound healing of HaCaT (a) and evaluation of scratch wound healing in % of uncovered area (b) [11].

**Conclusions**

The study's results strongly support that nanoceria-enhanced alginate–gum arabic cryogels are promising as advanced wound dressing. Favorable pore structure and moisture handling, matching key wound healing requirements. Biocompatibility and cellular support showed excellent results, with gradual release of nanoparticles, suggesting active involvement in the wound healing process.

## 3.3 Skeletal muscle regeneration using bioactive glass-alginate-cellulose composites

The article investigates the potential of bioactive glass–alginate–cellulose composite biomaterials for promoting skeletal muscle regeneration, an area of increasing interest due to the limited self-repair capacity of muscle tissue after volumetric muscle loss injuries. Bioactive glasses are known for their capacity to release therapeutic ions that can stimulate tissue repair and angiogenesis, while alginate and cellulose polymers provide a biocompatible and mechanically supportive scaffold network.

**Cross-linking of bioactive glass-Alg-cellulose composites**

Fourier-transform infrared spectroscopy (FT-IR) and X-ray diffraction (XRD) patterns confirmed the successful integration of all components and indicated the formation of chemical bonds between the inorganic glass phase and the biopolymer network.

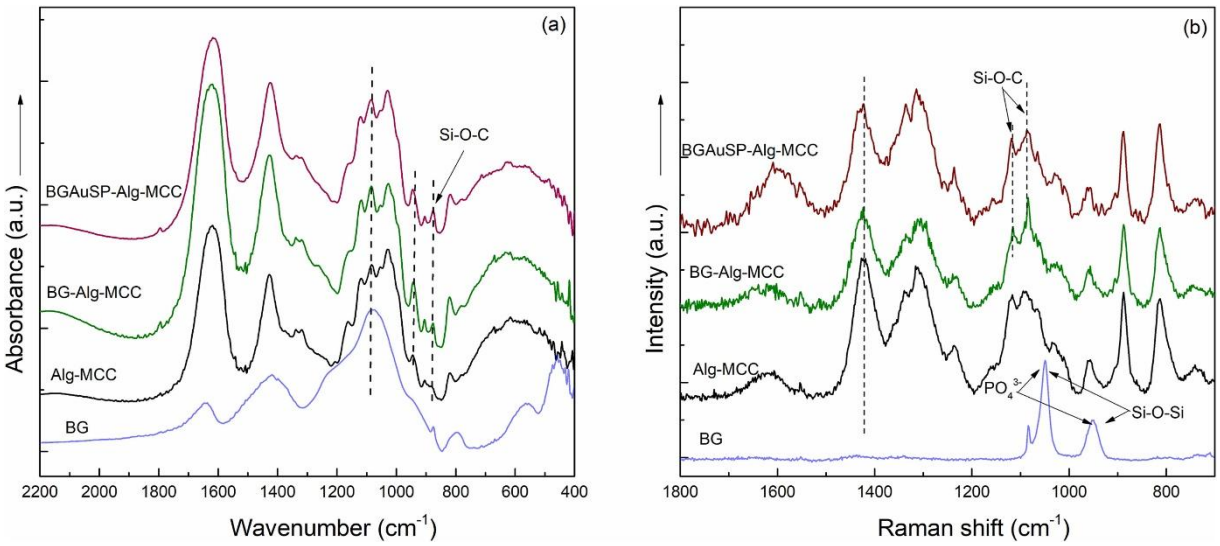


Figure 3.3.1 FT-IR (a) and Raman spectra (b) of BG (blue line), Alg-MCC (black line), BG-Alg-MCC (green line), and BGAuSP-Alg-MCC (burgundy line) composites [8].

Based on the cross-linking mechanism, which is taking place between MCC and Alg, and by the appearance of the Si-O-C vibration in composites, the triple composite is also confirmed. It needs to be mentioned that, thereby the cross-linking does not take place on the $COO^-$ group, the obtained composites are more favourable because they are taking place in different locations, by using other chemical groups.

A porosity of 80% was obtained for Alg, 97% for Alg-MCC composite, and 96% for BG-Alg-MCC and BGAuSP-Alg-MCC composites. Thus, with the addition of MCC, the porosity of the samples increases. In the SEM micrograph, these changes are evident, particularly the increase in pore size with MCC addition from 23 ± 2 to 53 ± 8μm (Figure 3.3.2). This may be due to several factors: i) the formation of ice crystals during the lyophilization process; and ii) the interaction between BGAuSP nanoparticles and the

crosslinking agent, $Ca^{2+}$ cations, which intervene in the polymer network and create more open structures, destroying the compactness; The largest pore size (97 ± 7μm) was obtained for the composite with BGAuSP.

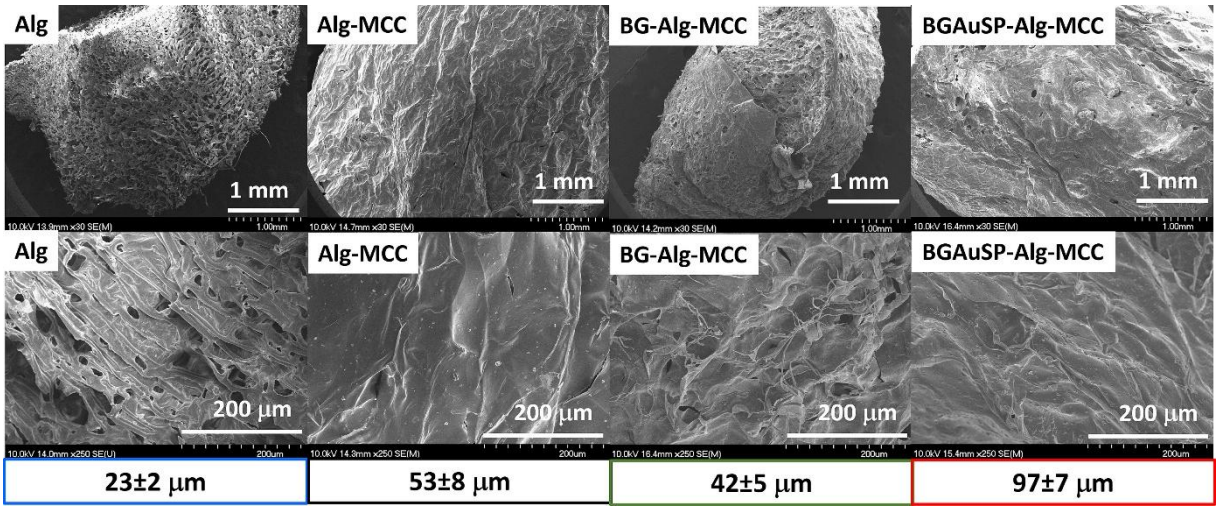


Figure 3.3.2 SEM micrographs of the Alg, Alg-MCC, BG-Alg-MCC, and BGAuSP-Alg-MCC composites. Scale bars: 1mm (first row) and 200μm (second row) [8].

**In vitro behaviour, biodegradation, and swelling ratio**

When immersed in simulated body fluid (SBF), the composites demonstrated bioactive behavior, evidenced by the formation of an apatite-like layer on the surface over time. This mineral layer is indicative of ionic dissolution from the bioactive glass and subsequent precipitation of calcium phosphate phases—an important interplay that enhances cell attachment and signaling for regeneration. Ions such as calcium and silicon were steadily released from the composite over extended periods, supporting sustained pro-regenerative signaling rather than a rapid burst release that can be detrimental to cell viability.

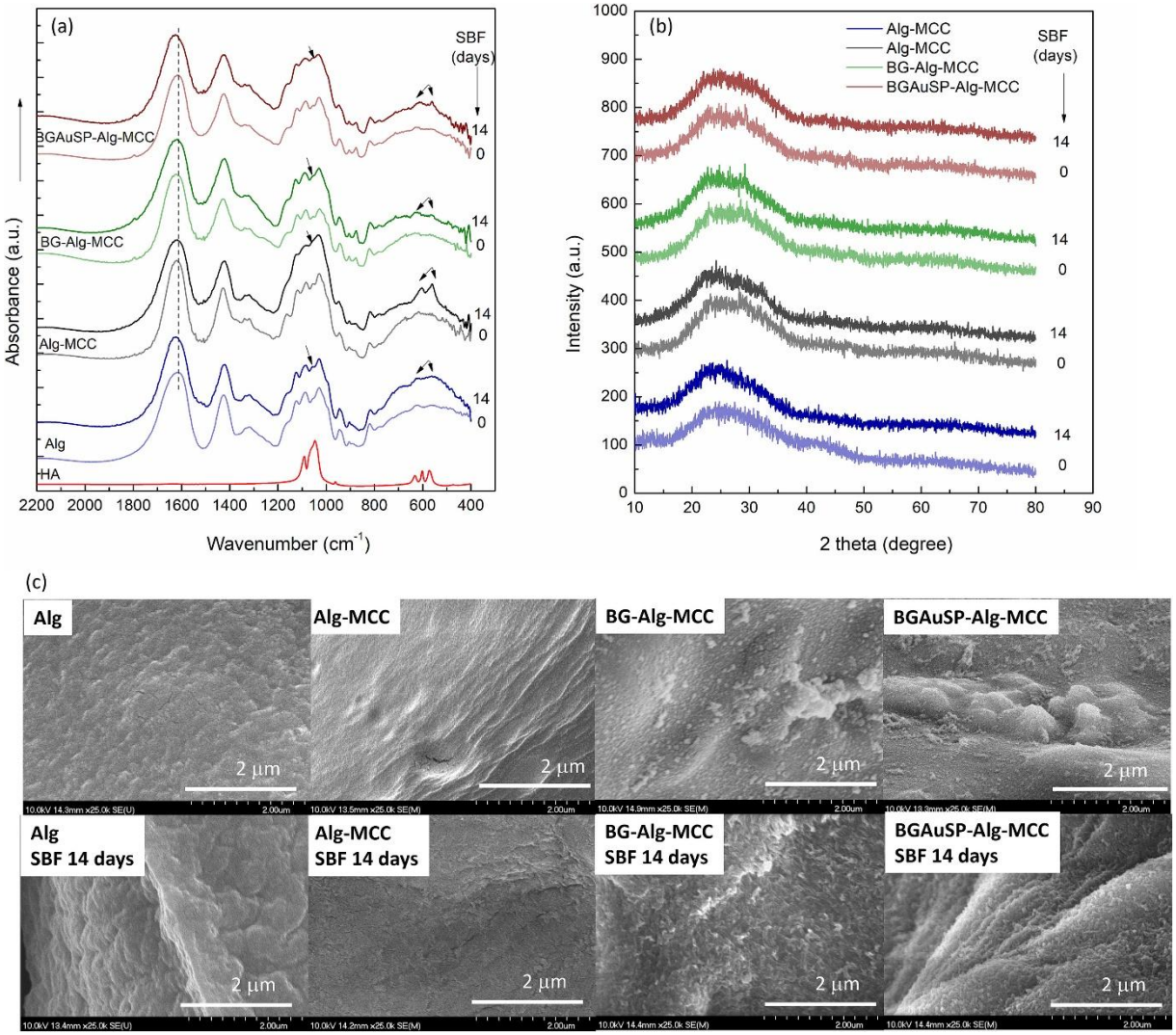


Figure 3.3.3 XRD pattern (a), FT-IR spectra (b), and SEM micrographs (c) of Alg (blue line), Alg-MCC (black line), BG-Alg-MCC (green line), and BGAuSP-Alg-MCC (burgundy line) before and after SBF immersion for 14 days. The FT-IR spectrum of hydroxyapatite (HA, red line) was inserted for comparison purposes. Scale bars: 2μm [8].

In vitro cytotoxicity assays confirmed minimal inflammatory response or cytotoxicity, further supporting the suitability of the composite for implantation. The gradual degradation and sustained bioactivity suggest that the scaffold maintains a balance between structural integrity and biological responsiveness that is critical for regenerative success.

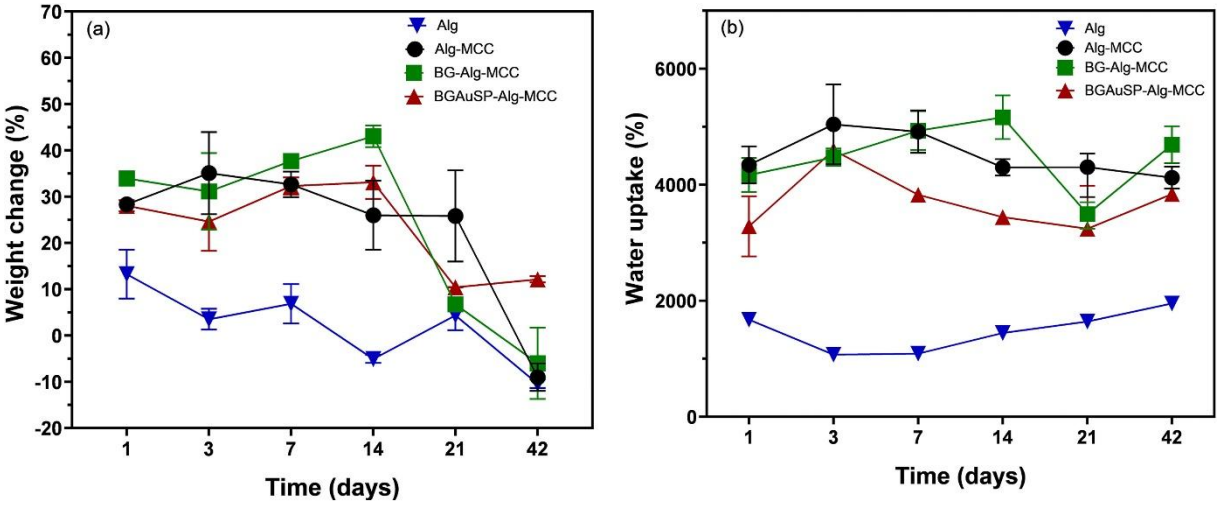


Figure 3.3.4 Degradation (a) and swelling ratio (b) of the Alg (blue line), Alg-MCC (black line), BG-Alg-MCC (green line), and BGAuSP-Alg-MCC (burgundy line) composite against degradation time. $P < 0.05$ [8].

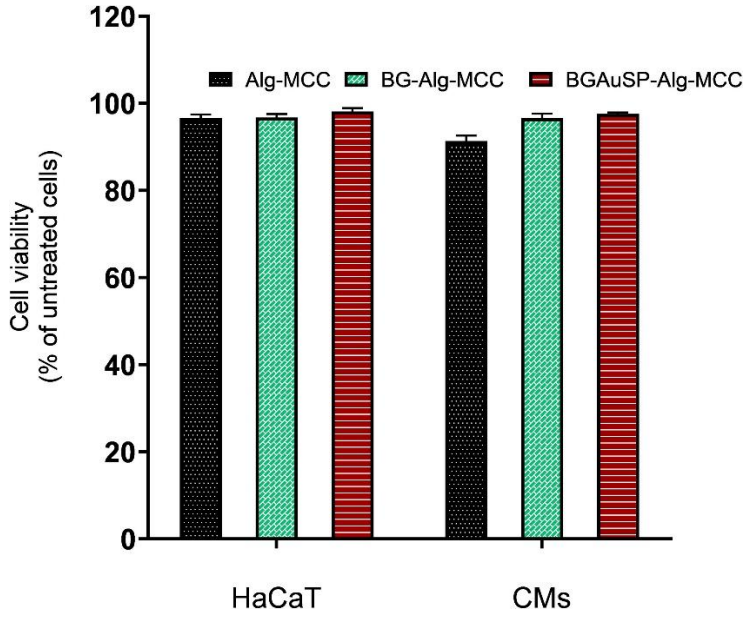


Figure 3.3.5 Viability of HaCaT and CMs cells after 24h interaction with Alg-MCC (black column), BG-Alg-MCC (green column), and BAuSP-Alg-MCC (red column) composites at the same concentration [8].

**Histological assessment of in vivo implanted biomaterials**

Compared MCC-Alg composites, the bioactive glass–integrated composites consistently outperformed in cell proliferation, differentiation potential, ion release profiles, and pro-angiogenic signaling. These differences highlight the synergistic effect of combining bioactive glass with natural biopolymers—leveraging the strengths of both inorganic and organic components to create a scaffold that better mimics aspects of physiological tissue environments.

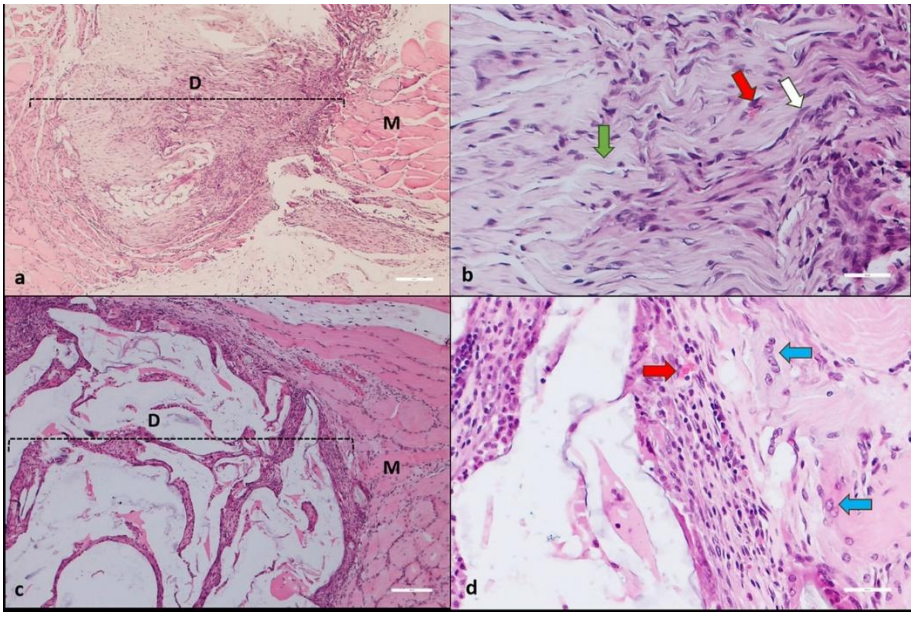


Figure 3.3.6 Histological evaluation of the tissue response in muscle defects at 2 weeks post-surgery in negative control (a, b) and treated (c, d) rats. In the control group, the muscle defect (D, marked area) was replaced with fibrous tissue composed of bundles of thick collagen fibers (green arrows), Hs (white arrow) and blood capillaries (red arrow); M indicates the skeletal muscle, H&E stain (a, b); In the treated group, the muscle defect (D, marked area) was occupied by the implanted material, containing mesenchymal cells, blood channels (red arrow), few collagen fibers, and mononuclear inflammatory cells. A few regenerating myofibers are seen at the periphery of the implanted material (blue

arrows); M indicates the skeletal muscle, H&E stain (c, d). The scale bar is 50μm (for a and c) and 10μm (for b and d), respectively [8].

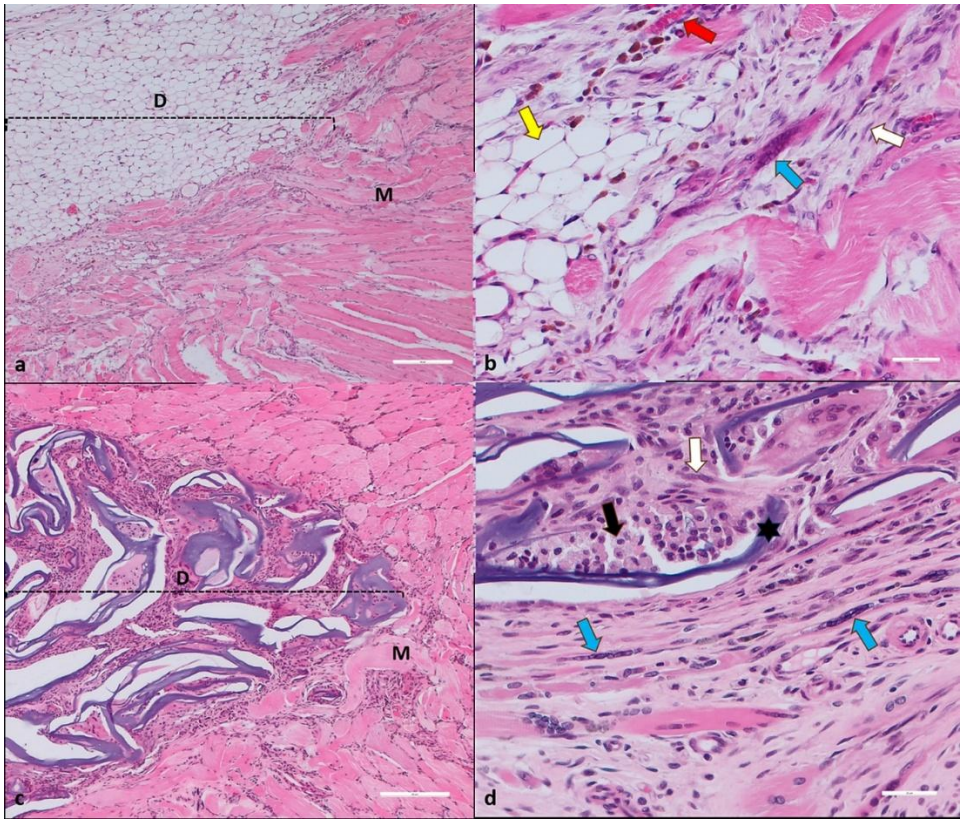


Figure 3.3.7 Histological evaluation of the tissue response in muscle defects at 4 weeks post-surgery in negative control (a, b) and treated (c, d) rats. In the control group, the muscle defect (D, marked area) was replaced with fibro-adipose tissue composed of clusters of adipocytes (yellow arrow), collagen fibers, and Hs (white arrow); few multinucleated myotubes (blue arrow) and blood capillaries (red arrow) are present at the periphery of the healed defect; M indicates the skeletal muscle, H&E stain (a,b); In the treated group, the muscle defect (D, marked area) is filled with fragments of implanted material (black asterisk), separated by mesenchymal cells (white arrow), blood channels, a few collagen fibers, and mononuclear inflammatory cells (black arrow). A significant number of multinucleated myotubes are seen at the periphery of the implanted material

(red arrows); M indicates the skeletal muscle, H&E stain (c, d). The scale bar is 50μm (for a and c) and 10μm (for b and d)[8].

**Conclusion**

Novel BG/BGAuSP-enhanced MCC-Alg composites were prepared by the ionic crosslinking method with calcium carbonate. In vitro experiments showed a non-cytotoxic effect on HaCaT and CMs cells, with cell viability values ranging between 96% and 98%. The in vitro behaviour of the samples was evaluated, and all samples showed the ability to develop an apatite layer that completely and homogeneously covered the composite surfaces after 14 days. Biodegradation tests revealed a notable finding: the introduction of cellulose into the Alg matrix significantly enhanced the degradation rate of the polymer, resulting in nearly 30 % mass loss after just one day of immersion. Furthermore, in vivo evaluation using a murine tibialis anterior VML model demonstrated that the biomaterial integrated well with the surrounding tissue with minimal collagen deposition and supported new myofiber formation during a 4-week implantation. Our findings demonstrate the potential of therapies for VML to enhance the regeneration and repair of the remaining musculature, underscoring their significant clinical relevance. The success of scaffold-based tissue regeneration depends on the development of biomaterials that establish a biocompatible and biomimetic microenvironment, fostering essential cell-material interactions and cellular functions such as proliferation and differentiation.

## Conclusions and Personal Contributions

Chapter 3.1 focuses on the development, optimization and characterization of cryogels obtained from Na-Alg and GA, with biomedical potential. The study showed that the interactions between the two polysaccharides, stabilized by calcium cations, lead to the formation of interconnected porous structures, whose

morphology and physicochemical properties depend on the proportion of GA. The internal structure is made up of interconnected pores (70–160 μm), and the proportion of GA significantly influences the size and uniformity of the pores. The composites demonstrated good absorption capacity, structural stability and bioactivity, highlighted by the formation of an apatite layer after immersion in SBF solution. Cytotoxicity tests confirmed good biocompatibility, with high cell viability (over 85–90%).

Personal contributions:

- Optimizing the ratio of polysaccharides that have a considerable influence on structural, morphological and biological properties.
- Development of a scheme for interpreting the process of calcium cation chelation in mixed polysaccharide matrices.
- Performing preliminary stability and absorption tests in aqueous media to evaluate the hydrophilic behavior of the composites.
- Performing a critical analysis of the results, identifying the strengths and limitations of the study and proposals for future research directions were formulated, such as expanding biological tests and integrating inorganic agents into the cryogel matrix.

Chapter 3.2 investigates the influence of cerium oxide nanoparticles (nanoceria) on the formation process, structure and biological behavior of com
posite cryogels obtained from Na-Alg and GA. It was demonstrated that the introduction of nanoceria modifies the crosslinking mechanism by creating additional interactions with the functional groups of polysaccharides, resulting in a more stable, porous and uniform network. Structural analyses (FT-IR, Raman, SEM) confirmed the formation of a homogeneous and resistant structure, and absorption tests indicated an increase of the fluid retention capacity, essential for wound

exudate management. In vitro experiments showed good biocompatibility and a pronounced antioxidant activity due to nanoceria, which contributes to reducing oxidative stress and accelerating the healing process. In conclusion, the inclusion of cerium oxide nanoparticles significantly improved the physicochemical and biological properties of the Alg–GA system, confirming the potential of this composite as an innovative material for bioactive dressings and tissue regeneration.

Personal contributions:

- Studying the crosslinking mechanism of the polysaccharide matrix (Alg + GA) following the inclusion of cerium oxide nanoparticles (nanoceria), to highlight the effect of the nanomaterial additive on the final structure.
- Evaluating the in vitro behavior of composites in the context of wound dressing: analyzing the absorption/biodegradation capacity, controlled release of nanoceria, support for cell growth (HaCaTs, Hs) and antioxidant potential (reduction of oxidative stress) in the context of healing.

Chapter 3.3 investigates the development of composite biomaterials for muscle tissue regeneration, obtained by combining Na-Alg and MCC with bioactive glass/gold nanoparticles. These were structurally and morphologically characterized, the results demonstrating a uniform, stable and bioactive porous network, capable of forming an apatite layer after immersion in SBF. The inclusion of bioactive glass significantly increased the degree of mineralization and bioactivity, and the addition of gold improved the cellular response. In vitro tests showed significant biodegradation, a good bioactive response, and an increase of the cell viability for muscle cells cultured on the surface of the composites. In vivo studies performed on a volumetric muscle tissue loss model confirmed the integration of biomaterials and stimulation of muscle regeneration through myofiber formation and vascular network development. The results indicate that these composites have significant

potential as bioactive supports for skeletal muscle tissue engineering. Overall, the research demonstrates that these composites based on Alg, cellulose and bioactive glass enhanced with Au agents represent promising materials for muscle tissue engineering applications and the treatment of severe muscle defects.

Personal contributions:

- Analyzing the formation and crosslinking mechanism of composites based on Alg, MCC and bioactive glass/Au, focusing on the interaction between the polysaccharide matrix and inorganic components.
- Interpreting structural and morphological characterization data (FT-IR, SEM, XRD) to highlight how the addition of bioactive glass and gold nanoparticles influences the morphology, porosity and stability of the composites.
- Evaluation of the correlation between the structure of scaffolds and their in vitro behavior, including degradation rate and apatite layer formation.

## List of papers related to the PhD thesis

1. Feraru, A.; Tóth, Z.-R.; Mureșan-Pop, M.; Baia, M.; Gyulavári, T.; Páll, E.; Turcu, R.V.F.; Magyari, K.; Baia, L. Anionic Polysaccharide Cryogels: Interaction and In Vitro Behavior of Alginate–Gum Arabic Composites. Polymers 2023, 15, 1844. https://doi.org/10.3390/polym15081844 (IF: 4.9, AIS: 0.657)
2. A. Feraru, Z-R. Tóth, K. Magyari, M. Baia, T. Gyulavári, E. Páll, E. Licarete, C. Costinas, O. Cadar, I. Papuc, L. Baia, The effect of nanoceria on the alginate-gum arabic crosslinking mechanism and in vitro behavior as a wound dressing. Int. J. Biol. Macromol., 288 (2025), 138569, 10.1016/j.ijbiomac.2024.138569 (IF: 8.5, AIS: 1.013)
3. A. Feraru, A. Zăvoi, K. Magyari, Z-R. Tóth, E. Bobu, E. Páll, A. Dreanca, A. Negoescu, M. Taulescu, M. Cenariu, M. Muresan-Pop, T. Gyulavári, I. Papuc, L. Baia, Skeletal muscle regeneration using bioactive glass-alginate-cellulose composites. Int. J. Biol. Macromol., 330 (2025), 148032, https://doi.org/10.1016/j.ijbiomac.2025.148032 (IF: 8.5, AIS: 1.013)

## List of other papers:

### ISI indexed

i) Magyari, K., Dreancă, A., Székely, I. et al. How does the structure of pullulan alginate composites change in the biological environment?. J Mater Sci 57, 19050–19067 (2022). https://doi.org/10.1007/s10853-022-07775-8

ii) Tóth ZR, Feraru A, Saszet K, Veréb G, Vodnar DC, Todea M, Timar-Gabor A, Dave AK, Sand D, Dreanca A, Magyari K, Baia L. Relation between shape-tailored $CeO_2$ nanoparticles morphology and hemocompatibility and antimicrobial effect. Biomater Adv. 171, 214229 (2025). DOI: 10.1016/j.bioadv.2025.214229.

### non-ISI indexed

i) Zs-R Tóth, K Magyari, A Feraru, I Szekely, L Nánai, A Dreanca, L Baia, Prediction Of The Antioxidant Character By Using Photocatalytic Activity Of Differently Shaped Cerium-Oxide Nanoparticles. Studia Universitatis Babes-Bolyai, Physica, 2023, Vol 68, Issue 1/2, p83, ISSN 0258-8730. DOI: 10.24193/subbphys.2023.08

## Conferences

### International:

a. *DPG Spring Meeting of the Condensed Matter Section 2025,* Regensburg, Germany 16-21 March, The effect of spherical nanoceria on the anionic polysaccharides and in vitro behavior as a wound dressing, Alexandra Feraru, Zsejke-Réka Tóth, Klára Magyari, Monica Baia, Tamás Gyulavári, Emőke Páll, Emilia Licarete, Codrut Costinas, Oana Cadar, Ionel Papuc, Lucian Baia, Poster

b. *8th China-Europe Symposium on Biomaterials in Regenerative Medicine (CESB 2024)*, Nuremberg, Germany, 15-18 September 2024, Cerium oxide nanoparticles incorporated into polymer matrices for soft tissue engineering, Alexandra Feraru, Zsejke-Réka Tóth, Monica Baia, Tamás Gyulavári, Emőke Páll, Klára Magyari, Lucian Baia, Poster

c. *The 15th International Conference on Physics of Advanced Materials (ICPAM-15)*, Sharm El Sheikh, Egypt, The influence of gum Arabic on physical and biological properties of alginate-based biocomposites, A. Feraru, Zs-R. Tóth, M. Mureșan-Pop, M. Baia, T. Gyulavári, E. Páll, R. V.F. Turcu, K. Magyari, Baia L. Baia, Poster

d. *33rd Conference of the European Society for Biomaterials, 4-8 September, 2023*, Davos, Switzerland, Biopolymeric Cryogels based on Alginate-gum arabic Polysaccharides as Biodegradable Macroporous Scaffolds, Alexandra Feraru, Zsejke-Réka Tóth, Alexandra Dreancă, Emma Bobu, Emilia Licarete, Lucian Baia, Klára Magyari, Poster
e. *32nd Conference of the European Society for Biomaterials, Bordeaux*, France, 4-8 September, 2022, Alginate-Based Biocomposites Hydrogels Reinforced with Natural Polymers Used in Tissue Engineering: Structural and Physicochemical Properties, Alexandra Feraru, Zsejke-Réka Tóth, Klára Magyari, Lucian Baia, Poster
f. *31st Conference of the European Society for Biomaterials*, Porto, Portugal, 5-9 September, 2021 *Online*, Comparative study between the effect of AgI and $Ag_2O$ on in vitro bioactivity and antibacterial activity, A. Feraru, Z.-R. Tóth M. Todea, D.-C Vodnar, K. Magyari, L. Baia, Poster

## Conference award:

a. *6th Autumn School on Physics of Advanced Materials (PAMS-6)*, November 19 – 26, 2023, Sharm El Sheikh, Egypt; *Sponsor's award* offered by APEL LASER for the short oral presentation entitled: In vitro evaluation of alginate-gum arabic hydrogel-based porous scaffolds loaded with cerium oxide nanoparticles, A. Feraru, Zs-R. Tóth, K. Magyari, Baia L. https://icpams.com/main/awards/

# Bibliography


[1] Chen Q, Zhu C, Thouas GA. Progress and challenges in biomaterials used for bone tissue engineering: bioactive glasses and elastomeric composites. Prog Biomater 2012;1:2. https://doi.org/10.1186/2194-0517-1-2.

[2] Arango-Ospina M, Boccaccini AR. Bioactive glasses and ceramics for tissue engineering. Tissue Engineering Using Ceramics and Polymers, Third Edition 2022:111–78. https://doi.org/10.1016/B978-0-12-820508-2.00019-2.

[3] Sergi R, Bellucci D, Cannillo V. A review of bioactive glass/natural polymer composites: State of the art. Materials 2020;13:1–38. https://doi.org/10.3390/ma13235560.

[4] Schiltz L, Grivetti E, Tanner GI, Qazi TH. Recent Advances in Implantable Biomaterials for the Treatment of Volumetric Muscle Loss. Cells Tissues Organs 2024;213:486–502. https://doi.org/10.1159/000536262.

[5] Nuge T, Liu Z, Liu X, Ang BC, Andriyana A, Metselaar HSC, Hoque ME. Recent advances in scaffolding from natural-based polymers for volumetric muscle injury. Molecules 2021;26. https://doi.org/10.3390/molecules26030699.

[6] Rodriguez Ayala A, Christ G, Griffin D. Cell-scale porosity minimizes foreign body reaction and promotes innervated myofiber formation after volumetric muscle loss. NPJ Regen Med 2025;10:12. https://doi.org/10.1038/s41536-025-00395-1.

[7] Loh QL, Choong C. Three-dimensional scaffolds for tissue engineering applications: Role of porosity and pore size. Tissue Eng Part B Rev 2013;19:485–502. https://doi.org/10.1089/ten.teb.2012.0437.

[8] Feraru A, Zăvoi A, Magyari K, Tóth ZR, Bobu E, Páll E, Dreanca A, Negoescu A, Taulescu M, Cenariu M, Muresan-Pop M, Gyulavári T, Papuc I, Baia L. Skeletal muscle regeneration using bioactive glass-alginate-cellulose composites. Int J Biol Macromol 2025;330:148032. https://doi.org/10.1016/J.IJBIOMAC.2025.148032.

[9] Feraru A, Tóth ZR, Mureșan-Pop M, Baia M, Gyulavári T, Páll E, Turcu RVF, Magyari K, Baia L. Anionic Polysaccharide Cryogels: Interaction and In Vitro Behavior of Alginate–Gum Arabic Composites. Polymers (Basel) 2023;15. https://doi.org/10.3390/polym15081844.

[10] Elhoudi M, Oukhrib R, A. Celaya C, G. Araiza D, Abdellaoui Y, Barra I, Brahmi Y, Bourzi H, Reina M, Albourine A, Abou Oualid H. Comparison of green bio-based cerium/alginate vs. copper/alginate beads: a study of vibrational and thermal properties using experimental and theoretical methods. J Mol Model 2022;28. https://doi.org/10.1007/s00894-022-05028-8.

[11] Feraru A, Tóth ZR, Magyari K, Baia M, Gyulavári T, Páll E, Licarete E, Costinas C, Cadar O, Papuc I, Baia L. The effect of nanoceria on the alginate-gum arabic crosslinking mechanism and in vitro behavior as a wound dressing. Int J Biol Macromol 2025;288. https://doi.org/10.1016/j.ijbiomac.2024.138569.

[12] Atisme TB, Yu CY, Tseng EN, Chen YC, Hsu PK, Chen SY. Interface interactions in conjugated polymer composite with metal oxide nanoparticles. Nanomaterials 2019;9. https://doi.org/10.3390/nano9111534.